Parameter dependence of dynamic D retention in W

-- Based on D. Nishijima et al., Nuclear Fusion 61 (2021) 116028.

Daisuke Nishijima, Russ P. Doerner, Matt J. Baldwin, George R. Tynan
Center for Energy Research, University of California San Diego, La Jolla, CA 92093-0417, USA

In-operando surface measurements during plasma exposure are required to explore dynamic retention.

- **Dynamic retention**, including both **solute (un-trapped) and "weakly" trapped D atoms**, is quickly released after the termination of the incident plasma flux.
  - Ex-situ analysis (e.g. TDS) is not appropriate.
- In-operando ion beam analysis (IBA), such as NRA, has been used to study dynamic retention in a couple of experiments so far.
- We have applied **LIBS (laser-induced breakdown spectroscopy)** for conducting in-operando surface measurements.
  - In comparison with IBA, an LIBS system is much simpler, and quicker measurements are possible.

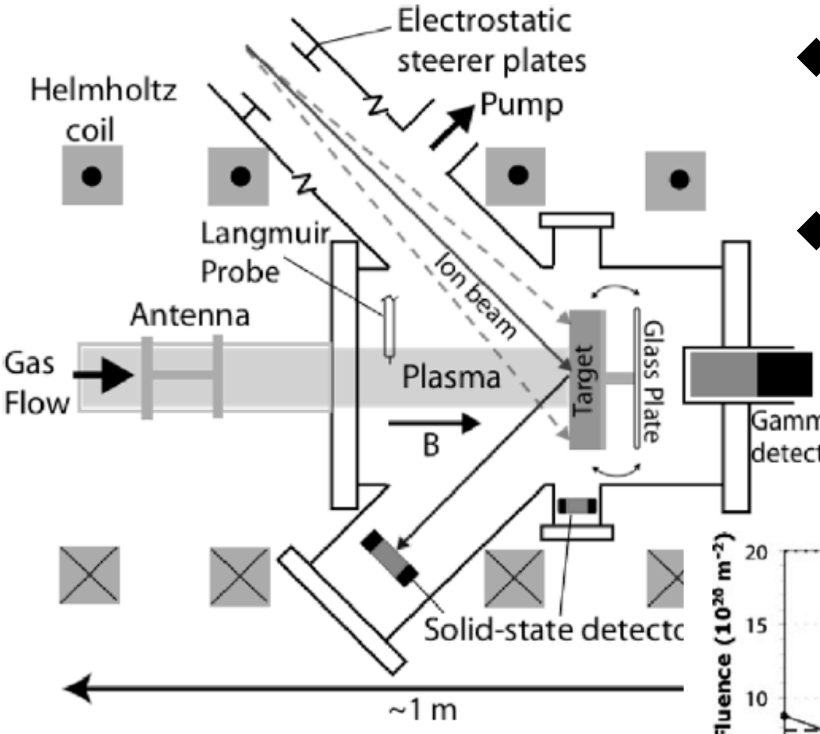

Fig. 1. A schematic of the DIONISOS experiment

- Example of NRA measurements during D plasma exposure of Mo in DIONISOS.
- Measurement depth ~ 5 μm.

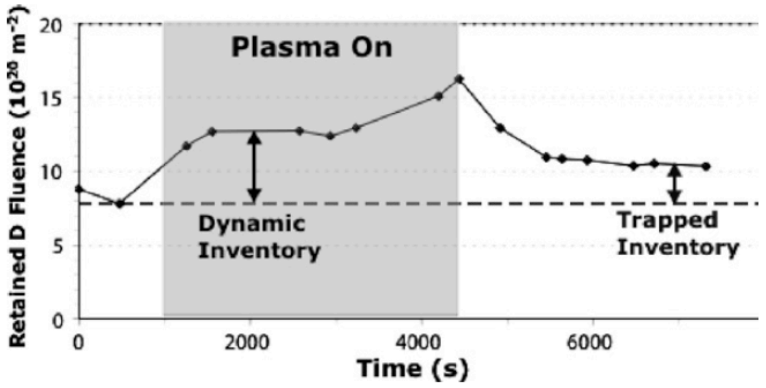

Fig. 4. NRA measured retained D fluence in the Mo plate in real-time; before, during, and after a deuterium plasma exposure with flux density of 1.8×10^{21} D/m^2 s and $V_{bias} = 100$ V.

T_s ~ 300 K

G.W. Wright et al., JNM 2007

An in-operando/in-situ LIBS system has been developed and upgraded in PISCES-A.

- Q-switched Nd:YAG laser (λ = 1064 nm, $\Delta t_L \sim$ 5 ns, $E_L \sim$ 115 mJ)
- A remote-controlled motorized mirror mount enables to quickly and accurately control the laser spot location.
- Echelle type spectrometer (Andor ME5000) + ICCD camera (Andor iStar DH334T): $t_{delay} \sim$ 10 ns & t_{width} = 2 μs
- Ablation depth: ~350 nm/shot & Spot diameter: ~150 μm
- The laser spot location was moved between each laser shot.
- 20 shots were accumulated to produce an emission spectrum for better statistics.
- Around 5 spectra were typically collected for each condition.
  - Mean value and uncertainty
- D I 656.1 nm/W I 429.4 nm intensity ratio is used to study dynamic D retention behavior in W.

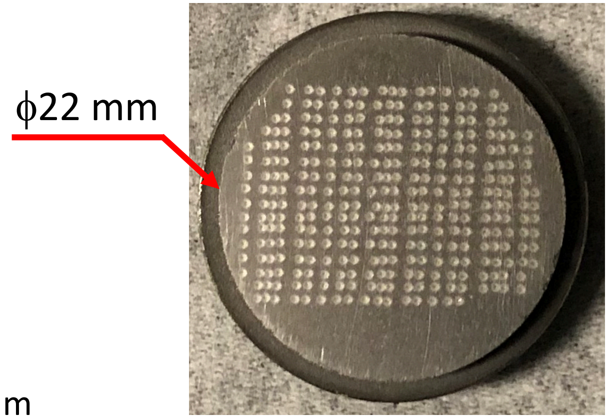

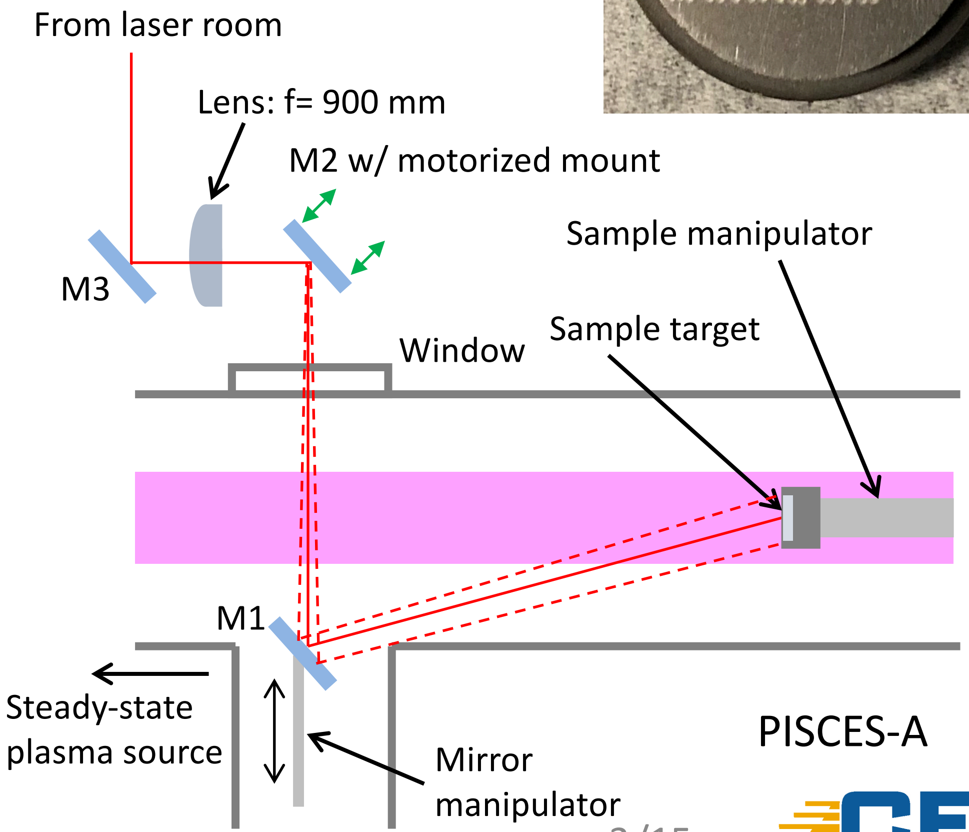

How can we extract the dynamic retention component from in-operando LIBS D_α signal during steady-state plasma exposure?

- The D_α line emission of in-operando LIBS measurements during steady-state plasma exposure can contain the following multiple components:

  - Background D/D_2 gas excited by steady-state plasma
    - ✓ D_α line emission was not detected due to the short t_{width} = 2 μs.
  - Ejected D atoms (dynamic and static retention) excited by steady-state plasma
    - ✓ Laser-induced plasma D_α emission is localized right on the W surface.
    - ✓ The steady-state plasma $n_e \sim 0.1\text{x}10^{18}$ m^{-3} is several orders of magnitude lower than that of typical laser-induced W plasmas.

  Negligible.

  - **Dynamic retention excited by laser-induced plasma**
  - Static retention excited by laser-induced plasma
  - Background D/D_2 gas excited by laser-induced plasma

The P_{D2} dependence reveals that there is no contribution of Bg gas to the LIBS signal during plasma exposure at $P_{D2} \leq 1.0$ mTorr.

- St was taken under vacuum, and is consistent.
- StBg linearly increases with P_{D2}.
- On the other hand, **DyStBg is nearly constant at $P_{D2} \leq$ 1.0 mTorr**, and increases with P_{D2} at > 1.0 mTorr.
- **There is no contribution of Bg gas to in-operando LIBS D_α signal during plasma exposure at $P_{D2} \leq 1.0$ mTorr.**
- Hard to quantify the Bg component at P_{D2} > 1.0 mTorr. → Not used in further studies.
- Note that no steady-state background plasma emission was detected even at P_{D2} > 1.0 mTorr.

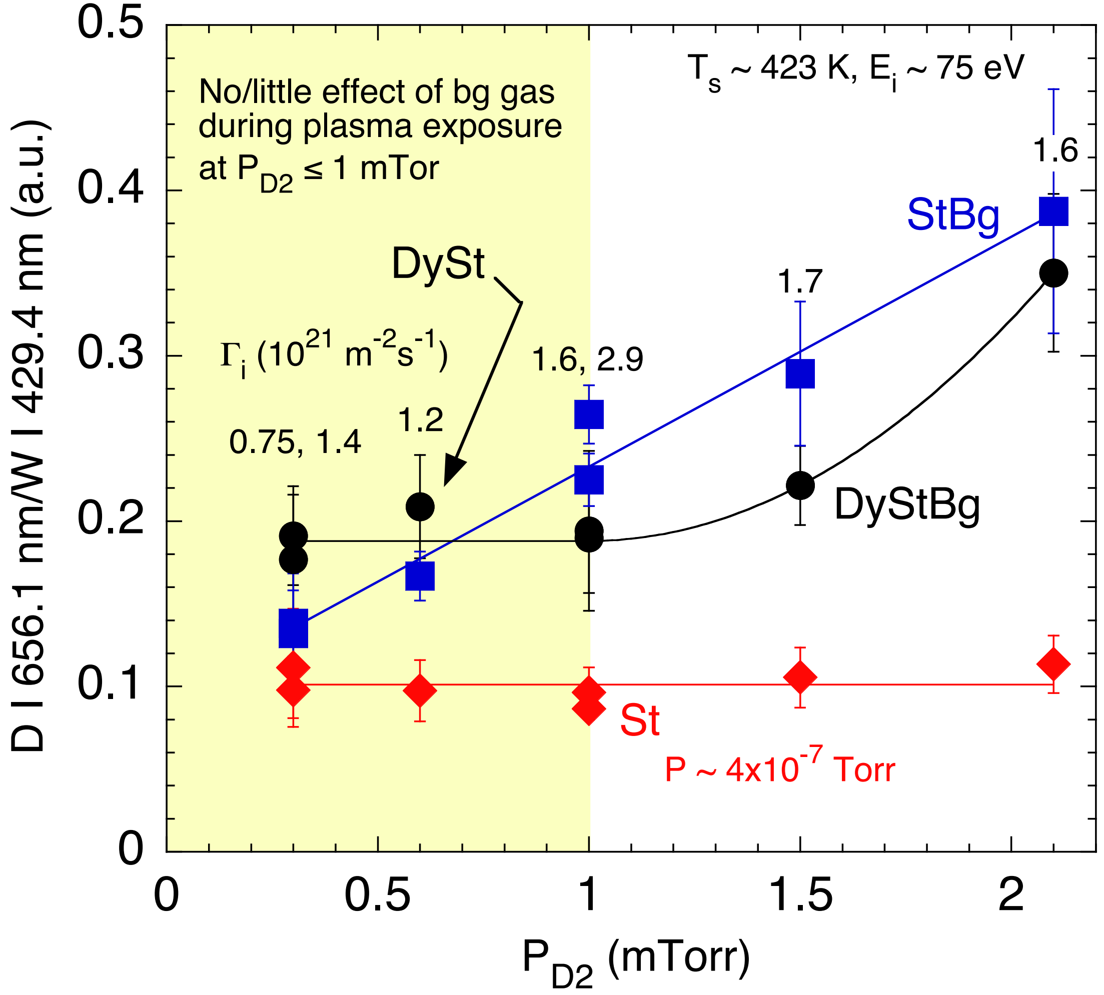

The dynamic retention component can be extracted from Dy = DySt ($P_{D2} \leq 1$ mTorr) – St (vacuum).

Plasma	Ambient background gas	LIBS signal can contain contributions from	Condition
During	$P_{D2} \leq 1$ mTorr	Dynamic + Static	DySt
After	$P_{D2} < 5 \times 10^{-7}$ Torr	Static	St

Dynamic retention: Dy = DySt ($P_{D2} \leq 1$ mTorr) – St (vacuum)

D/W atomic fraction can roughly be converted from D I/W I line ratio.

PISCES

- Laser ablation depth: ~ 350 nm
- Static D/W$_{St:SSL}$(0-10nm) ~ 0.1 in the near-surface layer at T_s ~ 300 K [1].
- Static D/W$_{St:PL}$(10-350nm) ~ 10^{-4} in a plateau region [2].
- $\int_{0\,nm}^{350\,nm} D/W_{St}\,dz$

  = D/W$_{St:SSL}$(0-10nm) x 10 nm + D/W$_{St:PL}$(10-350nm) x 340 nm

  = $0.1 \times 10 \times 10^{-9} + 10^{-4} \times 340 \times 10^{-9} \sim 1 \times 10^{-9}$ (**dominated by D/W in SSL**)

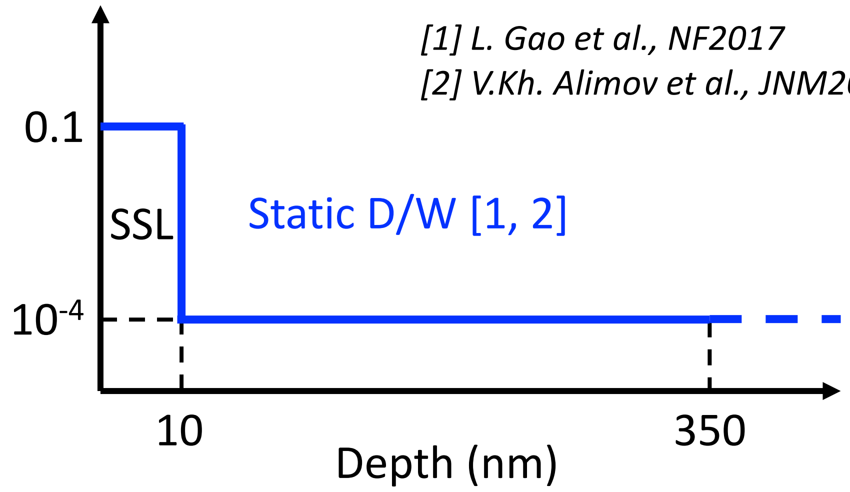

- **Dynamic retention is assumed to be localized in the near-surface layer.**
  - Dynamic retention can be negligible in the deeper region because of the low solubility of W.
- D I/W I intensity ratio: Dy ≈ St at T_s ~ 350 K (and $\Gamma_i \sim 0.9\times10^{21}$ m^{-2}s^{-1})
- $\int_{0\,nm}^{10\,nm} D/W_{Dy}\,dz \approx \int_{0\,nm}^{350\,nm} D/W_{St}\,dz$

  → D/W$_{Dy}$(0-10 nm) x 10 nm ≈ 1×10^{-9} → D/W$_{Dy}$(0-10 nm) ~ 0.1

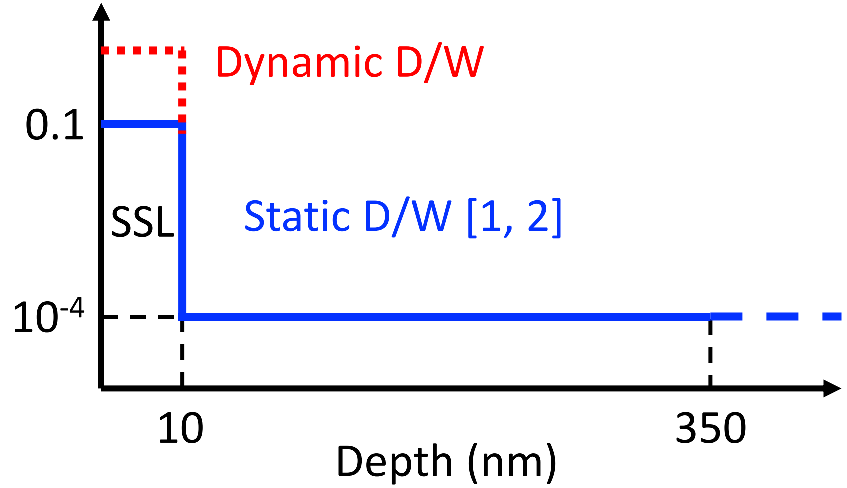

The behavior of dynamic retention of D in W is systematically explored, while varying the plasma exposure parameters.

- Apply the conversion factor (D/W ~ 0.70 x D I/W I) to the following parameter dependence study.

- **Incident ion energy, E_i, dependence**: $E_i \sim 45 – 175$ eV

- **Sample temperature, T_s, dependence**: $T_s \sim 348 – 573$ K

- **Incident ion flux, Γ_i, dependence**: $\Gamma_i \sim 0.26\times10^{21} – 2.9\times10^{21}\ m^{-2}s^{-1}$
  - A low flux range because of $P_{D2} \leq 1$ mTorr

In each parameter scan, the other parameters were kept as constant as possible.

- **Effect of He bubbles**
  - Sequential plasma exposure from pure He to pure D

Measured dynamic D retention in W depends on T_s and Γ_i, while no/little E_i dependence is observed.

PISCES

- No clear E_i dependence of all three components is seen in the range of $E_i \sim 45 – 175$ eV.
- All three components monotonously decrease with increasing T_s.
- The T_s dependence of Dy is stronger than that of St.
- Dy linearly increases with increasing Γ_i, and saturates at $\Gamma_i \geq 0.75\text{x}10^{21}\ \text{m}^{-2}\text{s}^{-1}$.
- DySt (St) only slightly increases (decreases) or both are nearly constant with increasing Γ_i.

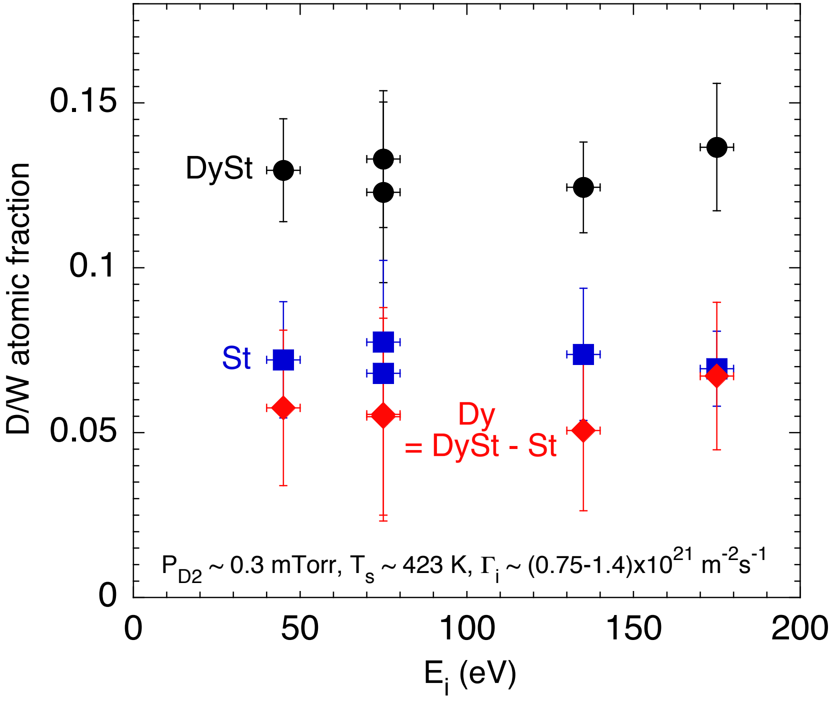

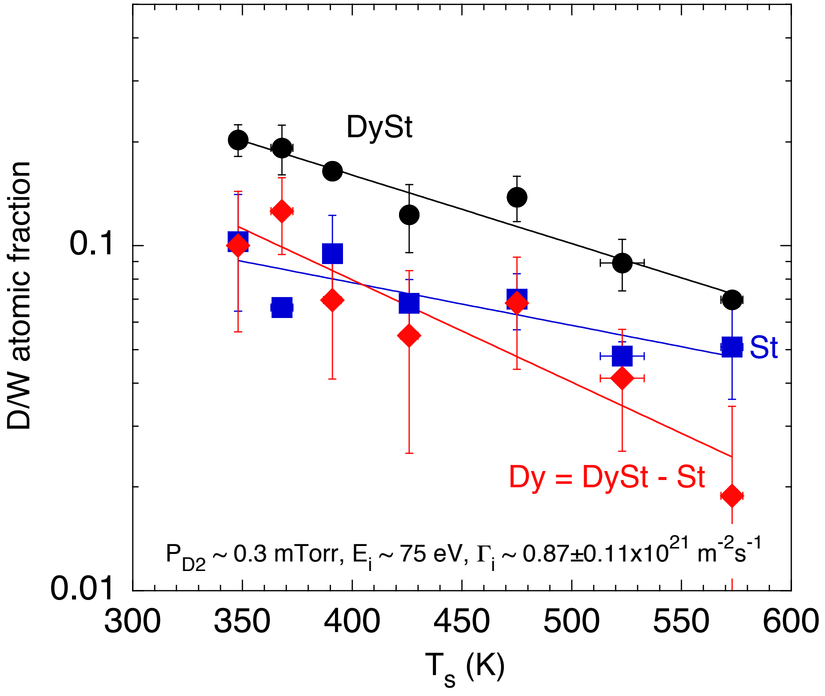

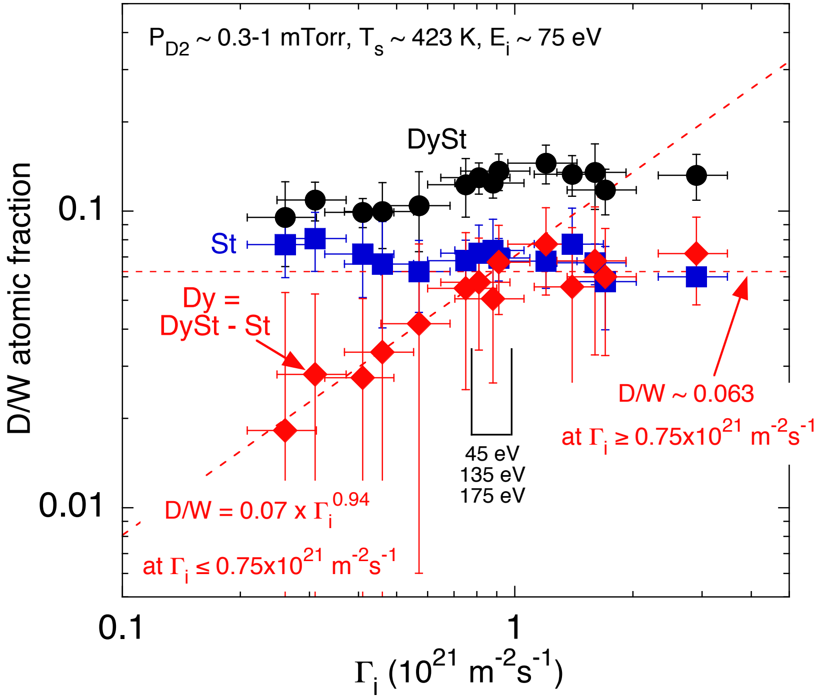

Observed trends on E_i and T_s are qualitatively consistent with a global model prediction (E.A. Hodille et al., PRM 2018).

- The global model assumes two kinds of "trapping" sites: **interstitial sites** and **single vacancies** (with various VH_x).
- The global model predicts that **H atoms trapped in single vacancies are dominant** over solute H in the total retention, **when an SSL is formed**.
- In our experiments, **the amount of dynamic retention is comparable to that of static retention**.
  - In addition to solute H, "**weakly" trapped H atoms in vacancies (E_t < 1 eV?) should/may also be treated as dynamic retention.**
  - **LIBS cannot distinguish solute and weakly trapped D atoms.**

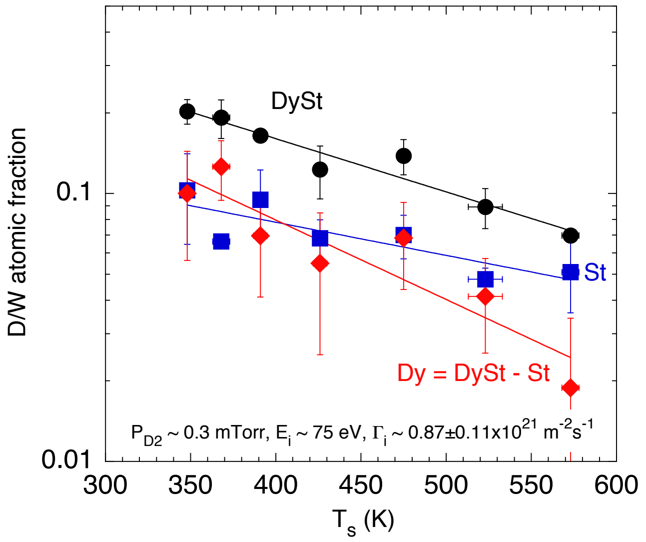

- The T_s dependence of Dy is observed to be stronger than that of St.
  - **De-trapping energies of solute & weakly trapped D (dynamic retention) are lower than those of strongly trapped D (static retention).**

- The model prediction is qualitatively consistent with our observed trends on E_i and T_s for both dynamic (Dy) and total (DySt) retention.
  - **The very weak or no E_i dependence** and **the decreasing retention with increasing T_s.**

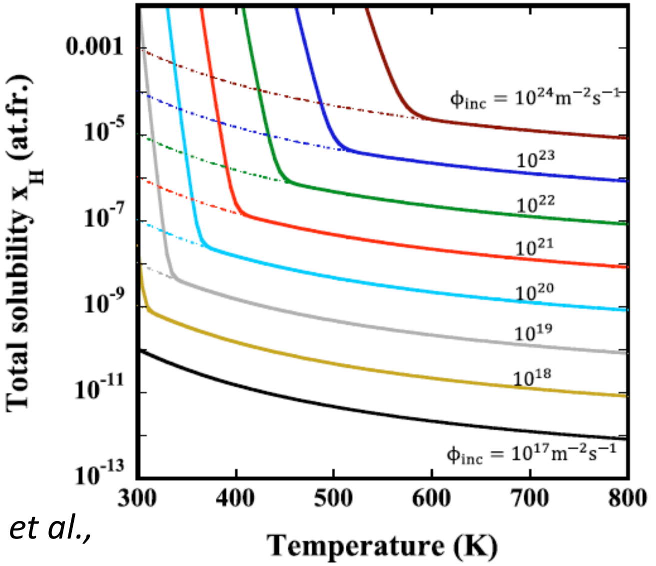

E.A. Hodille et al., PRM 2018

There is a discrepancy between our measurement and the global model prediction in the Γ_i dependence.

PISCES

- DySt (St) only slightly increases (decreases) or both are nearly constant with increasing Γ_i.
- Dy saturates.
  - May interstitial & trapping sites saturate with D?
  - May diffusion/recombination/reflection properties effectively change with the high fraction of D?

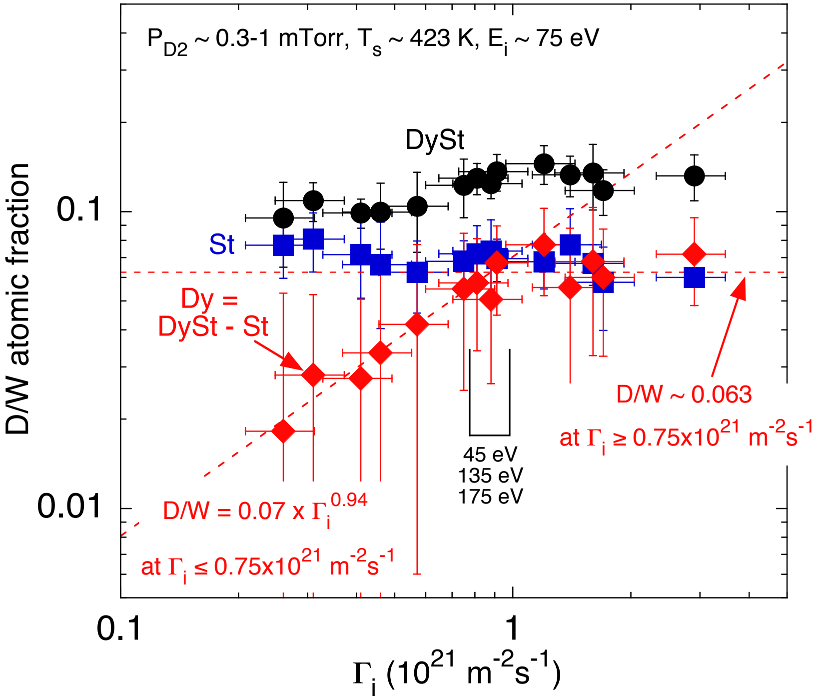

- The model predicts a strong increase of the total retention with an increase in Γ_i.
- Does the total retention saturate?

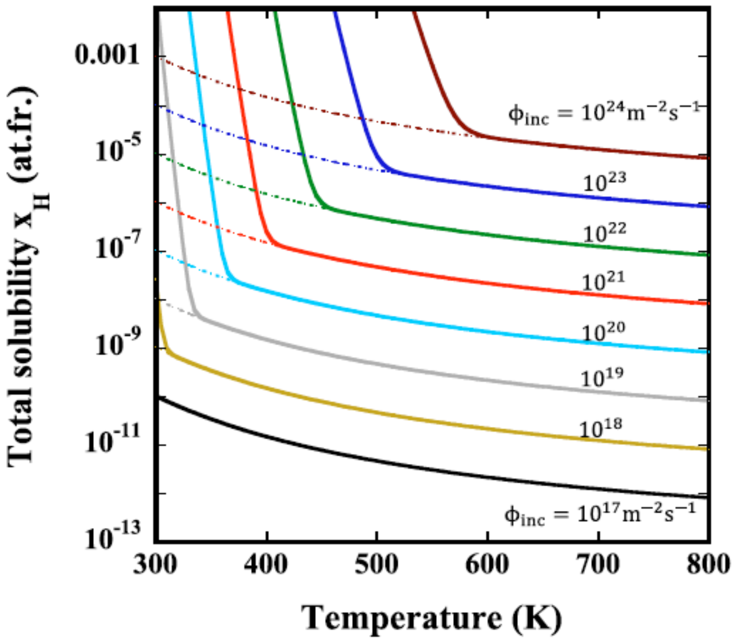

FIG. 4. Total solubility of hydrogen (bold lines) implanted at Rp for various incident fluxes ranging from $\phi_{inc} = 10^{17}$ to 10^{24} m^{-2} s^{-1} plotted as a function of the temperature of implantation and for an incident energy of $E_{inc} = 500$ eV/ion. The fraction of hydrogen trapped at interstitial sites is also plotted in dotted lines for comparison.

E.A. Hodille et al., PRM 2018

MD simulations show stress-induced H self-trapping in W (R.D. Smirnov and S.I. Krasheninnikov NF 2018).

- Initially **perfect bcc W lattice** is assumed.
- No change in W lattice and H behavior at interstitial H/W ≤ 1 at.%.
- **At interstitial H/W = 10 at.%, H atoms quickly start to agglomerate into multiple platelets.**
- **H self-trapping** phenomenon leads to the spontaneous formation of platelets.

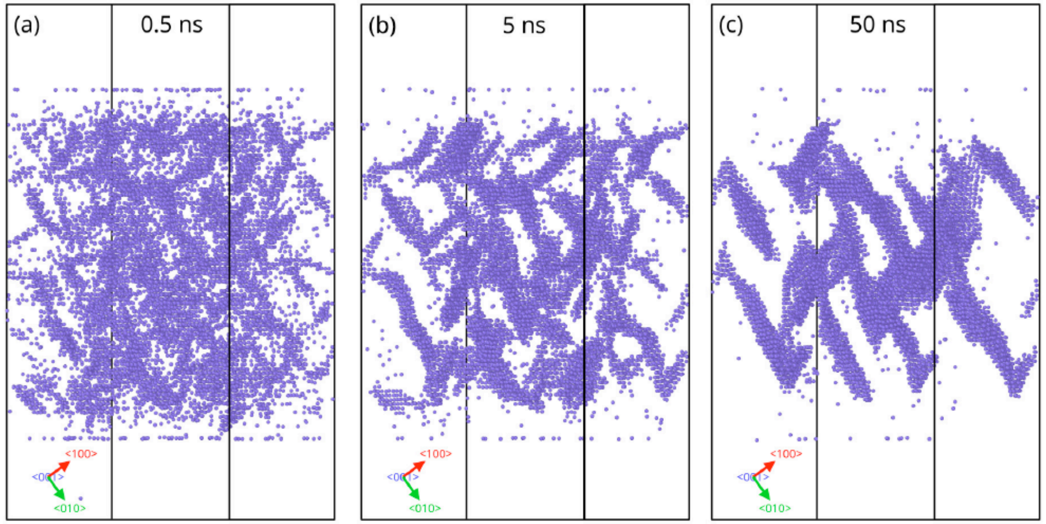

Figure 3. Platelet-like structures of self-trapped hydrogen atoms (purple dots) forming at 10 at.% hydrogen density in the initially perfect bcc tungsten lattice at 0.5 ns (*a*), 5 ns (*b*), and 50 ns (*c*) simulated time. The black lines represent edges of the simulation box. The vector tripod indicates principal directions of the initial bcc tungsten lattice. Color in this figure is available on-line.

- With **a pre-existing dislocation, lower interstitial H/W = 0.3-1 at.%** are enough to form **self-trapped H** structures (platelet).

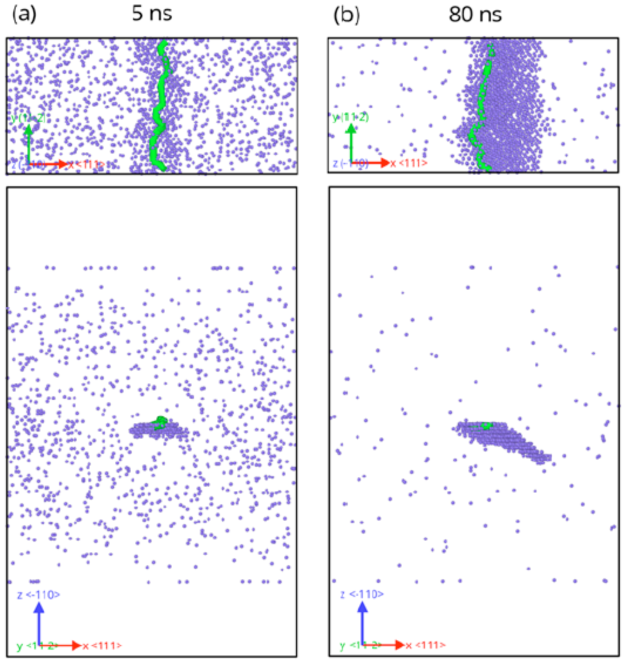

Figure 4. Top and front views of spatial distribution of hydrogen atoms (purple dots) near the edge dislocation (green line) in tungsten sample with 1 at.% hydrogen at 5 ns (*a*) and 80 ns (*b*) simulated time. The vector tripod shows coordinate system used in the simulations. Color in this figure is available on-line.

- De-trapping energy of H atoms from a platelet.

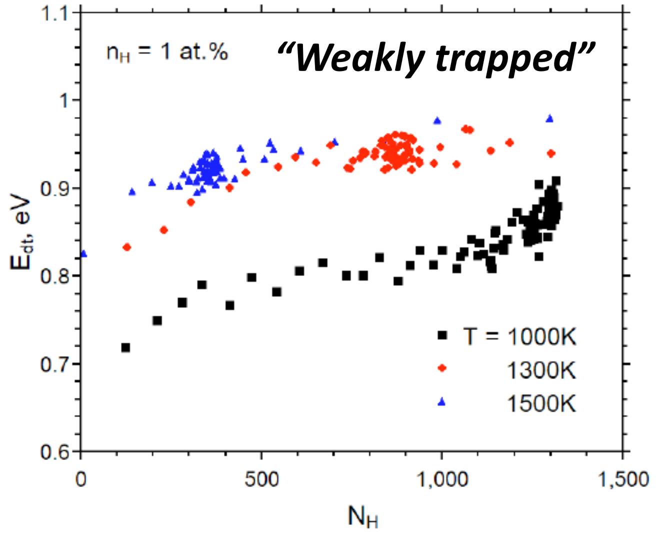

Figure 12. The evaluated hydrogen atom de-trapping energy from the platelet-like structure formed near the edge-dislocation as function of the number of hydrogen atoms in the structure for the different system temperatures. Color in this figure is available on-line.

- ***This stress-induced H self trapping mechanism can also contribute to the surface super-saturation.***

Dynamic D retention in W is not strongly affected by He bubbles in the near-surface region.

- First, a W target was exposed to pure He plasma at T_s ~ 773 K to produce He bubbles in the near-surface region.
- Then, the W target was exposed to pure D plasma at T_s ~ 423 K.
- **Dynamic retention is not strongly affected by He bubbles in the near-surface region.**
- Static retention in the near-surface region slightly increases with increasing He fluence.
  - **D atoms can be trapped around He bubbles** *[e.g. S. Markelj et al., NF2020]*.

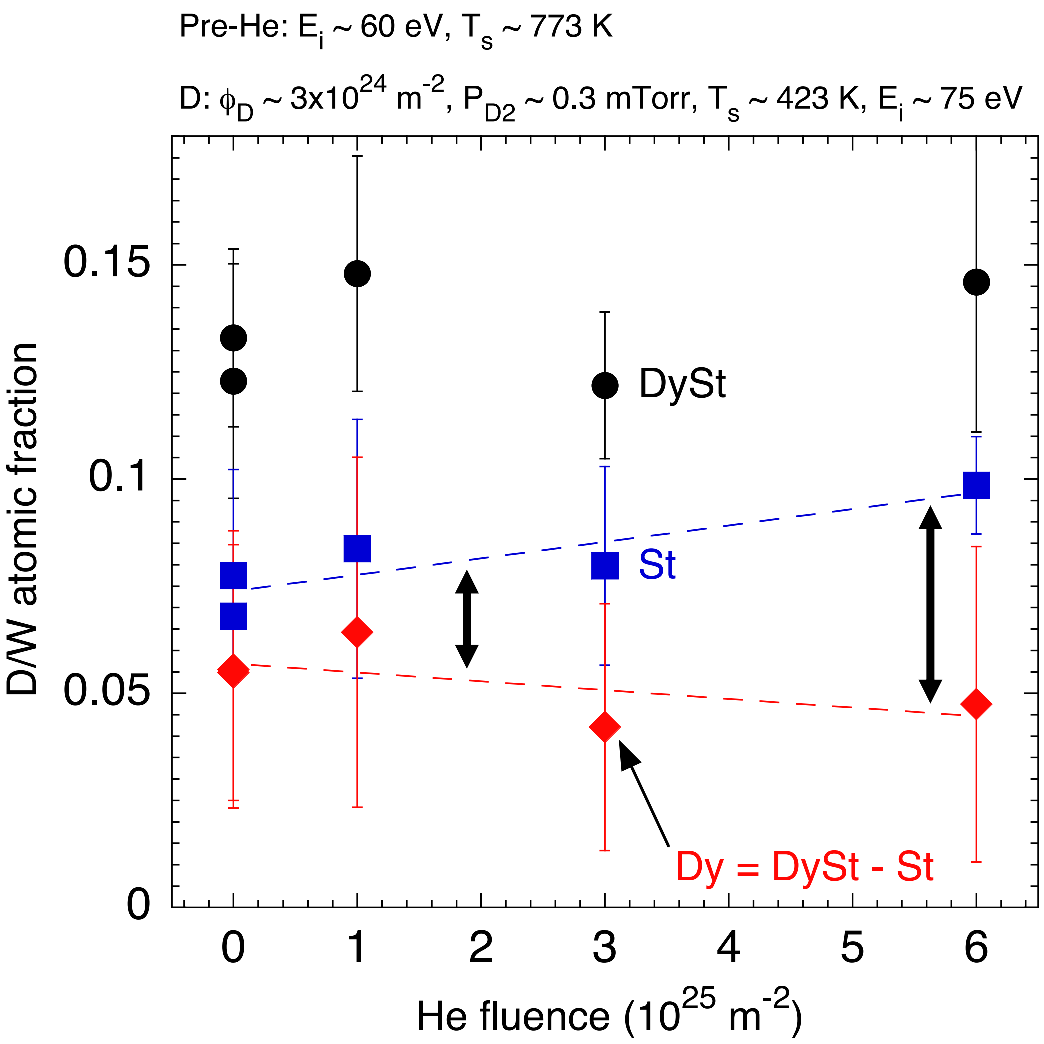

D retention properties of W during plasma exposure have been investigated in PISCES-A using the in-operando LIBS system.

PISCES

- **E_i** dependence
  - **No clear dependence of Dy, St, and DySt in the range of E_i ~ 45 – 175 eV**.
  - Qualitatively consistent with the global model prediction and the MD simulation.
- **T_s** dependence
  - **Dy, St, and DySt monotonously decrease with increasing T_s at ~ 348 – 573 K.**
  - Qualitatively consistent with the global model prediction.
  - T_s dependence of Dy is stronger than that of St.
    - → Lower de-trapping energies of solute and weakly trapped D atoms (Dy).
- Γ_i dependence
  - **Dy linearly increases with increasing Γ_i, and saturates at $\Gamma_i \geq 0.75 \times 10^{21}$ $m^{-2}s^{-1}$**.
  - **DySt (St) only slightly increases (decreases) or both are nearly constant with increasing Γ_i.**
  - Inconsistent with the global model prediction.
- Effect of **He bubbles**
  - **Dy (St) only slightly decreases (increases)**.

Ex-situ analyses of supersaturated layer will be performed using FIB/TEM and GDOES.

PISCES

- Layer thickness and (relative) D amounts vs. E_i, T_s, and Γ_i.

- GDOES depth profiling of RAFM steel samples was done.
  - Depth resolution: ~ 0.125 nm.
  - D signal (Ly_α at 2nd order) was successfully detected in a Cr-rich surface layer.

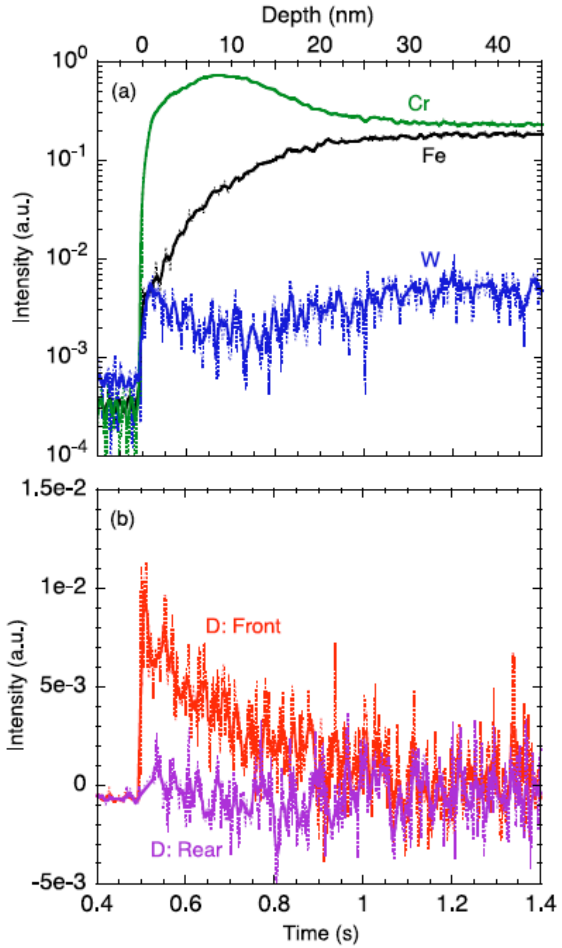

D. Nishijima et al., NME 2021

Fig. 5. GDOES depth profile measurements of CLAM 19–05: (a) Fe, Cr, and W in the plasma-exposed (front) surface in a semi-logarithmic scale, and (b) D in both front and rear surfaces in a linear scale. The thick solid lines exhibit smoothed data with a smoothing width of 5 data points, while the dotted lines show raw data. The depth is calculated with 50 nm s^{-1}, based on the total sputtering time of 200 s and the measured crater depth of ~ 10 μm.

UC San Diego

CER Center for Energy Research